International Journal of Technology 10(2): 236-246
ISSN 2086-9614

PREDICTING THE MOTIONS OF A FISHING BOAT CAUSED BY IMPROVING THE STERN PART USING A HYBRID PARTICLE-GRID SCHEME

Suandar Baso[1*], Hidemi Mutsuda[2], Yasuaki Doi[2]

[1]*Naval Architecture Department, Faculty of Engineering, Hasanuddin University, Jl. Perintis Kemerdekaan Km.10, 90245, Makassar, Indonesia*
[2]*Division of Energy and Environmental Engineering, Faculty of Engineering, Hiroshima University, 1-4-1 Kagamiyama, Higashi-Hiroshima, 739-827, Hiroshima, Japan*

(Received: September 2018 / Revised: November 2018 / Accepted: March 2019)

ABSTRACT

Improving a ship's stern part could help to reduce greenhouse gases and costs. However, a ship sailing in actual conditions experiences disturbances that can affect its performance. Ship performance is an important aspect of the design process that guarantees ship safety. The heave and pitch motions of an improved fishing boat were predicted numerically by using a hybrid scheme of Eulerian grid-Lagrangian particle, hereinafter improving its stern part and attaching an additional part. The stern part improvement and additional structure attachment affected an increase on the heave amplitude from the ship's basic form by 5% to 10%. Moreover, the improvement of the stern part in the bottom area contributed to a better heave amplitude than that of the side area. Finally, the pitch amplitude for all forms was relatively small and affected an increase of 5% to 9%, dependent on the form. The improvement had a greater effect on heave motion than pitch

Keywords: Additional structure attachment; Heave motion; Hybrid particle-grid scheme; Pitch motion; Stern part improvement

1. INTRODUCTION

Energy efficiency has drawn global attention to the decarbonizing of economies, the securing of energy supplies, and the increasing of productivity. This attention has involved the marine engineering field as well. To reduce ships' greenhouse gas emissions, the International Maritime Organization (IMO) has urged the Marine Environment Protection Committee (MEPC) to identify and develop mechanisms to achieve such a reduction (IMO, 2010). To this end, the MEPC has introduced regulations focused on the limitation of CO_2 production of newly built ships (MEPC, 2011). Optimization of the hull form and appendages are necessary to match these targets, which were both elaborated on by Legovic & Dejhalla (2016). This means that a ship's geometry should be optimized appropriately due to its significant relation to ship performance and energy efficiency.

The resistance reduction improvements on the bow part of a fishing boat have been carried out by multiple researchers, such as Miyata et al. (1981), Miyata and Doi (1984), Suzuki et al. (1992), Kawashima et al. (2003) and Masuya (2007). However, few have been concerned with improvement on stern end bulb of Japanese fishing boats. Kim and Yang (2013), along with

[*]Corresponding author's email: s.baso@eng.unhas.ac.id, Tel. +62-411-586015, Fax. +62-411-586015
Permalink/DOI: https://doi.org/10.14716/ijtech.v10i2.2354

Gabor (2011), have recently conducted numerical works related to stern part improvement to reduce drag, and Supriadi et al. (2015) applied a replication of micro-riblets to a ship's hull for drag reduction. That being said, the styles of fishing boats are known to vary as widely as fishing techniques.

Mutsuda et al. (2013) studied the numerical resistance reduction of fishing boats by improving the stern part. In this study, the improvement of the body line and the addition of a structure at the stern part was examined to reduce drag resistance. All of the cases proposed in this study could reduce water resistance with the maximum reduction rate of around 15 to 20% when compared with the ship's basic form (original case). In addition, Suastika et al. (2017) studied the effects of a stern foil application on ship resistance by using a numerical method and comparing experimental results. Based on the results, applying a stern part foil to decrease ship resistance obtained an effect at high speed ($Fr \geq 0.5$), decreasing ship resistance up to 10.0%. By contrast, properly designed bulbous bows have been proven to reduce resistance by 15% to 40%, depending on the steaming speed, overall hull proportions, etc. (Friis et al., 2010; Friis et al.,2017).

Shenglong et al. (2018) optimized the hull form of a ship in waves, based on a CFD technique, but, the motions of pitch and heave were not computed and only the ship motion was facilitated by the CFD technique. Kim et al. (2010) also optimized a hull form for reduced resistance and improved seakeeping via practical design-oriented CFD tools. In this paper, resistance reduction is clearly explained and obtained. However, the evaluation of seakeeping using the Bales' Ranking method could only quantify one wave condition (Kim et al., 2010). The improvement of ship form, such as that of fishing boats, must also contribute to good performance in a seaway, forcing designers to improve ship performance, such as reducing ship response or motion. Therefore, we continue the study (Mutsuda et al., 2013) by focusing on the motions of fishing boats as result of stern part improvement using a hybrid scheme or hybrid Eulerian grid with Lagrangian particle scheme. The improvement of the stern part in the bottom area enhances the heave amplitude while the pitch amplitude for all forms is relatively small and increases by 5% to 9%, depending on the form. Some snapshots caused by nonlinear interactions between ship-wave could be captured clearly.

2. METHODS

2.1. Overview of Hybrid Scheme

In a previous work (Baso et al., 2011b), a Eulerian scheme with Lagrangian particles was developed. Figure 1 shows an illustration of just such a Eulerian scheme with Lagrangian particles for computing a multiphase flow. This method possesses hybrid techniques, coupling a grid-based method (based on the constrained interpolation profile method) with particle-based method (based on the smoothed particle hydrodynamics (SPH) method). The SPH method could conserve mass and compute pressure from the weighted contributions of neighboring particles, allowing the direct creation of a free surface for two-phase interacting fluids. The constrained interpolation profile method is associated with solving advection equations in the advection phase, the first of the three stages in the time stepping procedure to solve nonlinear wave-body interaction problems. Density function ϕ_i (i = 1: gas, i = 2: water, i = 3: solid) is defined on the node of an Eulerian grid in all phases. The time evolution of the density function is advanced by the advection equation of ϕ_i. To compute an accurate interface between different phases, two kinds of Lagrangian particles having the density function ϕ_p are employed on an Eulerian grid in which physical values are defined on a staggered grid system. The time integration of free surface particles is computed using the fourth Runge-Kutta method. These free surface particles

and SPH particles can contribute to the correction of density function ϕ_i numerical errors coming from time integration on an Eulerian grid.

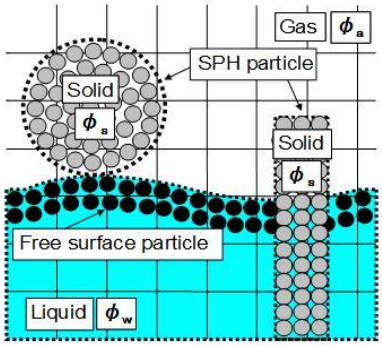

Figure 1 Illustration of an Eulerian scheme with Lagrangian particles (ϕ_i indicates the density function and the Lagrangian particles are located on Eulerian grids)

2.2. Governing Equations

The governing equations (Equations 1–3) for the fluid phase consist of the mass conservation equation, an incompressible Navier-Stokes equation, the equation of continuity, the density function for *i*-phase and its advection equation. The equations computed by a grid-based method are expressed as follows:

$$\frac{\partial \bar{u}_i}{\partial x_i} = 0 \tag{1}$$

$$\frac{\partial \bar{u}_i}{\partial t} + \bar{u}_j \frac{\partial \bar{u}_i}{\partial x_j} = -\frac{1}{\rho}\frac{\partial \bar{P}}{\partial x_i} - \frac{\partial \tau_{ij}}{\partial x_j} + \frac{\mu}{\rho}\frac{\partial^2 \bar{u}_i}{\partial x_j \partial x_j} + g_i + \bar{F}_{fsi} \tag{2}$$

$$\frac{\partial \phi_I}{\partial t} + \bar{u}_j \frac{\partial \phi_I}{\partial x_j} = 0 \tag{3}$$

where u_i is the velocity, μ is the coefficient of fluid viscosity, ρ is the fluid density, P is the pressure, F_{fsi} is the fluid-structure interaction, g_i is the acceleration due to gravity, τ_{ij} is the subgrid-scale (SGS) stress term, and ϕ is the density function. To reduce the model parameters, the SGS stress term is solved by using the dynamic SGS model. It is also used to represent the effect of unresolved small-scale fluid motions. A time-splitting technique is then employed for the multiphase flow. More details are provided by Mutsuda et al. (2008). Meanwhile, the governing equations for the solid phase are a continuity equation (Equation 4) and momentum equation (Equation 5) computed by the SPH method as follows:

$$\frac{D\rho}{Dt} + \rho\frac{\partial u^i}{\partial x^i} = 0 \tag{4}$$

$$\rho\frac{Du^i}{Dt} = \frac{\partial \sigma^{ij}}{\partial x^j} + g^i - F^i_{fsi} \tag{5}$$

where ρ is the density, u_i is the velocity, $P = -\sigma_{kk}/3$ is the position vector of vector *j* components, σ_s^{ij} is the stress tensor of the solid phase, and F_{fsi} is the fluid structure interaction term.

The pressure, with specified jump conditions, is solved by Poisson's equation (Equation 6) given by

$$\nabla \cdot \left(\frac{\nabla P^{n+1}}{\rho^*} \right) = \frac{\nabla \cdot u^*}{\Delta t}$$

(6)

where * denotes a physical value after the advection step. The pressure for the solid phase can be obtained by this equation and applied when solving a solid deformation.

The fluid structure interaction F_{fsi} is solved by acceleration obtained from the pressure on the SPH particles interpolated using the pressure on the grids solved by Equation 6. In the model, the fluid structure interaction F_{fsi} (Equations 2 and 5) can be given by the following equation:

$$F_{fsi}(\mathbf{r}_a) = -\frac{1}{\rho(\mathbf{r}_a)}\sum_b m_b \frac{P(\mathbf{r}_b)}{\rho(\mathbf{r}_b)}\nabla_a W(\mathbf{r}_a - \mathbf{r}_b, h) \tag{7}$$

where m_b is the particle mass, W is the Kernel function, r_a and r_b are the particle positions, and h is the radius of the referenced area where the interaction between particles can be considered. A ship's motion can be solved by using information obtained from SPH particles because a ship's hull consists of SPH particles capturing the motion and deformation of a ship. Therefore, to avoid the gimbal lock phenomenon, the three-dimensional (3D) motion of a ship hull is represented by describing the translation and rotation of a ship hull's center of gravity by using the quaternion given by the following equations:

$$\frac{\partial^2 x_{s,k}}{\partial t^2} = \frac{F_{s,k}}{m_i} - F_{fsi} \tag{8}$$

$$I\frac{\partial \omega_i}{\partial t} = T_i \tag{9}$$

$$\frac{\partial \theta_i}{\partial t} = \omega_i \tag{10}$$

where θ_t is the rotational angle, ω_t is the angular velocity, T_i is the torque, I is the inertia moment, and F_{fsi} is the fluid structure interaction. In addition, the center of gravity of a ship hull can be obtained by solving the inertia moment of SPH particles, which is calculated by using Baraff theory (1997). Based on this theory, the equations for 3D motion are given by

$$r_g = \frac{1}{N}\sum_{i=1}^{n} r_i \tag{11}$$

$$I = \frac{1}{N}\sum_{i=1}^{n} m\left|r_i - r_g\right|^2 \tag{12}$$

where N is the coordinate of the center of gravity of the rigid body, r_g is the position of the gravity center, I is the inertia moment, r_i is the position of the SPH particle i, and m is the mass of the particle.

The time integration of a ship's position is defined as follows:

$$\hat{r}_i' = \hat{r}_i^{k+1} - r_i^k \tag{13}$$

$$r_g^{k+1} = \frac{1}{N}\sum_{i=1}^{N} \hat{r}_i^{k+1} \tag{14}$$

$$\theta' = \omega dt = \frac{1}{I}\sum_{i=1}^{N} m\hat{r}_i' x(r_i^k - r_g^{k+1}) \tag{15}$$

$$r_i' = r_g' + R^{-1}(r_i^k - r_g^{k+1}) \tag{16}$$

where R^{-1} is inverse of the rotation matrix.

Therefore, the coordinates of velocity of each SPH particle in every time step can be tracked by using the rotation matrix and the amount of the angle rotation of the center of gravity.

3. VALIDATION

The developed numerical method of Eulerian grid-Lagrangian particle (Baso et al., 2011b; Mutsuda et al., 2013) had been validated previously with several cases, particularly regarding fishing boat and tanker motions in a nonlinear wave. The validations possess good agreement between numerical and computation results. In this section, the validation results have been explained for the tanker case. The tanker speed was set to 0.875 m/sec or the *Fr* number (0.1385) initially. The dimensions of the tanker model for the experimental work were 4.0m length (L_{pp}), 0.645 m width (B), and 0.258 m draft (d) (Baso et al., 2011b). The incident wave height was set to H_w/L_{pp} = 0.02 and the wave length was ranged from λ/L_{pp} = 0.25 to 1.25.
Figure 2 shows a comparison of the transfer functions of the heave and pitch motions between numerical, experimental, and strip theory results. Based on Figure 2, the computation of heave motion is consistent overall with the experimental result, but the computational result is relatively higher and overestimated in range $\sqrt{\lambda/L}$ 1.1 to 1.8. The overall comparison errors between the computational and experimental results for heaving motions are shown to be relatively small, with large errors only in $\sqrt{\lambda/L}$ 1.1 and 1.24. The averaged comparison error is 12%. Moreover, the comparison error between the computational and strip theory results for heaving motions averages 15%. For pitching motion, the overall value difference between computational and experimental results is significantly small and the averaged comparison error is 9%. In addition, the comparison error between computational and strip theory results averages 12%.

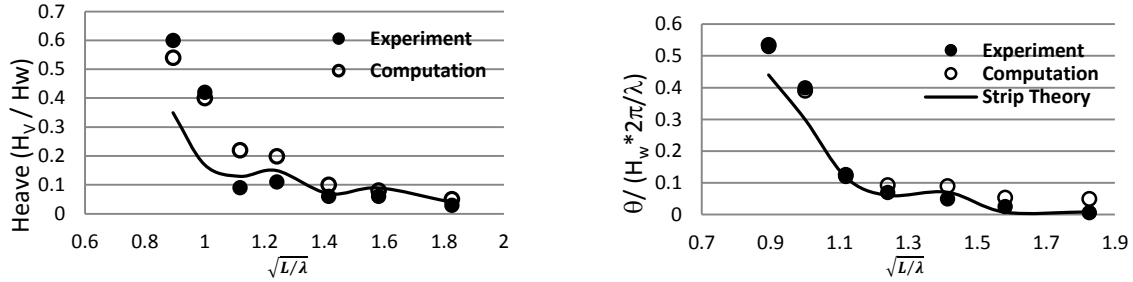

Figure 2 Transfer function of heave motions and pitch motions of the tanker

This can be interpreted as showing the heave motion increasing moderately with increasing wave lengths, but the experimental and strip theory tendencies fluctuate. The computation of pitch motion is very consistent with the experimental result as well.

4. RESULTS AND DISCUSSION

The larger low-pressure area, vortices flow and resultant forward water motion cause substantial energy loss and inefficiency. These are some reasons to improve the stern part and attach an additional structure on the stern part. Thus, the stern part improvements attempted to cause no

significant change on the ship's water line length, the quiet clearance for propeller installation, and the transom immersion reduction.

The principal particulars of the fishing boat model run in the computations are given in Table 1 and the body line plan of the fishing boat is shown in Figure 3. The 3D basic form is provided in Figure 4. The improved stern part is named Stern1 and Stern2. Then, the additional structure attachment are named Stern End Bulb 2 or SEB2, SEB2down, and SEB3. Stern1 has a trapezoidal shape on the rear main deck to the bottom vertically, whereas Stern2 has a shorter immersed transom shape than the basic form, as shown in Figure 5. SEB2 has an additional structure attached on the stern part with a width that is 89% of the ship's breath (B). The structure is located 65% of ship draft (d) vertically from baseline. SEB2down is located near corner of transom shape about 39% *d* vertically from baseline. SEB3 is a combination of SEB1 and SEB2. These are shown in Figure 6.

They were performed in a numerical water tank. The grid size was normalized by length between perpendiculars (Lpp) of 0.0025～0.015L_{pp} and the radius of free surface particles was 0.00125 ～0.005L_{pp}. Then, the radius of the SPH particle was 0.00125L_{pp}. For wave conditions, the incident wave height was set to H_w/L_{pp} = 0.06 and categorized as a high wave. The wave length was ranged from λ/L_{pp} = 0.5 to 2.0. Finally, the fishing boat speed was set to Fn = 0.384 initially.

Table 1 Principal particulars of the fishing boat model in the computational condition

Lpp (m)	1.5000
Lwl (m)	1.6492
B (m)	0.3066
L/B	4.8920
Cb	0.7155

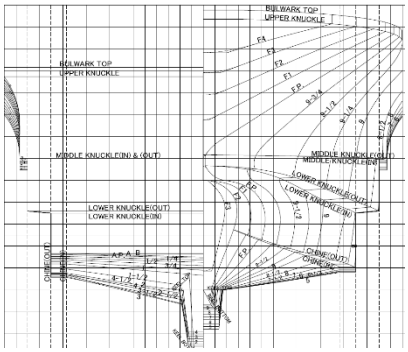

Figure 3 The body lines of the fishing boat

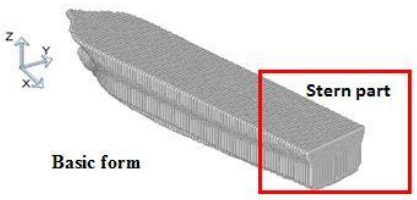

Figure 4 3D basic form

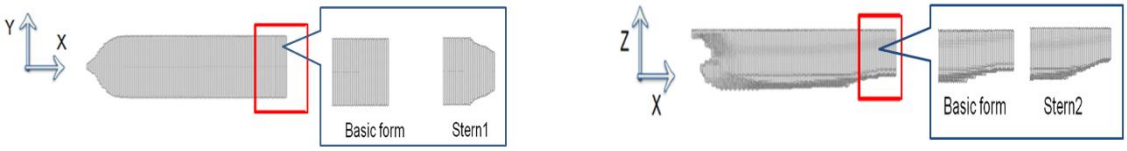

Figure 5 The improved stern part of Stern1 (left) and Stern2 (right)

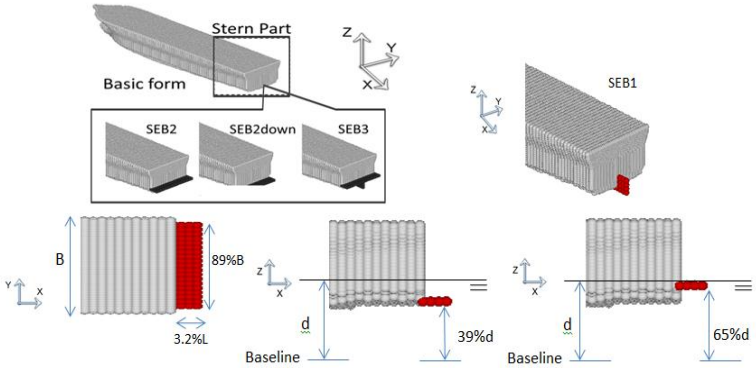

Figure 6 The additional structure attachment on stern parts SEB1, SEB2, SEB2down, and SEB3

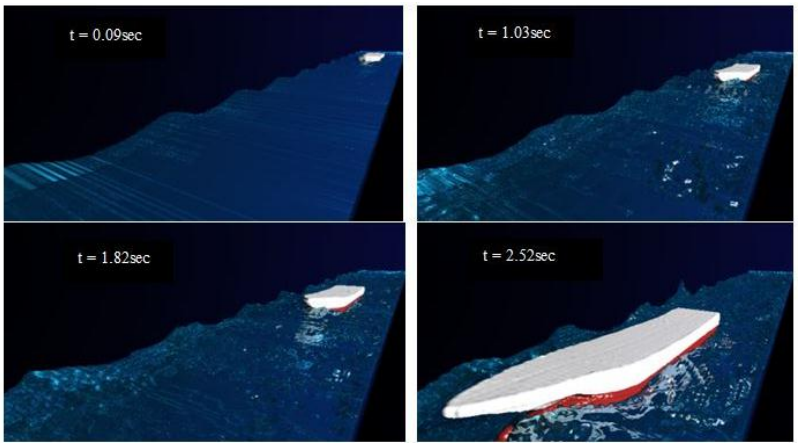

Figure 7 Snapshots of the basic form's motions in a heading wave (Fr = 0.384, λ/L_{pp} = 1.2, H_w/L_{pp} = 0.06)

Figure 7 shows some snapshots of the basic form acting gently in a heading wave. The length of the numerical wave tank was made longer to obtain several cycles of motion. From these snapshots, the occurrence of some phenomena caused by the interaction between the ship and the wave can be seen, such as water splashing near bow part and bow slamming.

Only the heave and pitch motions are considered, as the other motions are fixed. Figures 8 and 9 show the time history of the heave and pitch amplitudes, respectively. The amplitudes during the time period are fairly stable. In interpreting the motions of the fishing boat, the heave and pitch motions have been normalized. Non-dimensional heave is defined by H_v/H_w, and the pitch is defined by $\theta/(H_wK)$ where H_v and θ are the respective heave and pitch motion amplitudes, H_w is the incident wave height, and K is the wave number.

Figures 10 and 11 show the non-dimensional heave motions for each stern part improvement and additional structure attachment, respectively. From the figures, the heave motion tendency of all forms is identical, showing the heave motion tends to increase with the increasing wave length. The stern part improvement, shown in Figure 5, and the additional structure attachment, as shown in Figure 6, affect increases on the heave amplitude of the basic form by approximately 5% to 10%. The amplitude value is given by averaging a difference Response Amplitude Operator (RAO) of heave motion between the stern part improvements (Stern1 and Stern2) and the additional structure attachments (SEB2, SEB2down, and SEB3) with the basic form, as shown in Table 2. This means that the heave amplitudes of the stern part improvements and the additional structure attachments are higher than the basic form. However, the increase in heave motion is not significantly higher from λ/L_{pp} = 0.5–1.0 and 1.8–2.0.

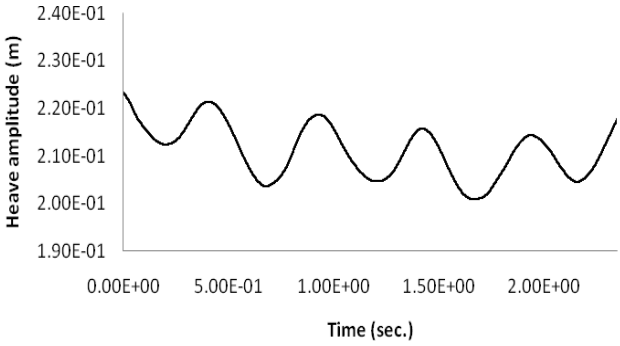

Figure 8 Time history of heave amplitude of Stern1 (Fr=0.384, λ/L$_{pp}$=1.2, H_w/L_{pp}=0.06)

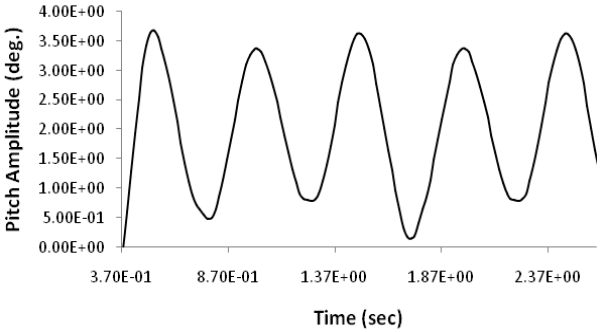

Figure 9 Time history of pitch amplitude of Stern1 (Fr=0.384, λ/L$_{pp}$=1.2, H_w/L_{pp}=0.06)

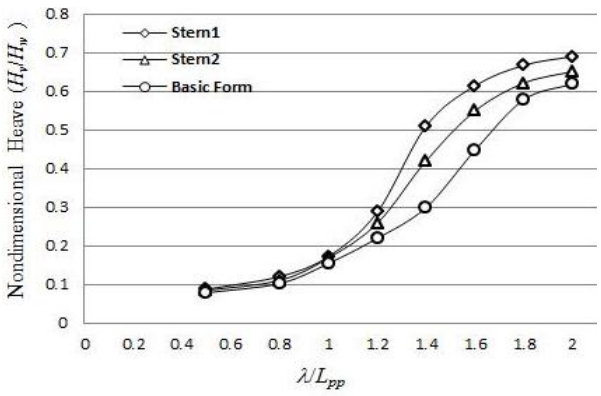

Figure 10 Non-dimensional heave motions of each stern part improvement

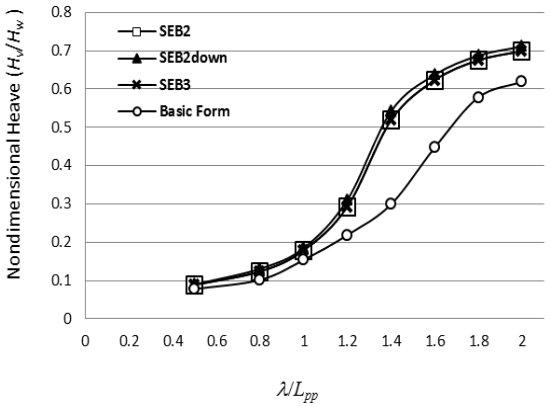

Figure 11 Non-dimensional heave motions of each additional structure attachment

Table 2 The RAO of heave motion

λ/L$_{pp}$	RAO Heave Motion					
	SEB2	SEB2down	Stern1	Stern2	Basic Form	SEB3
0.5	0.089	0.09	0.087	0.084	0.078	0.089
0.8	0.124	0.131	0.12	0.110	0.102	0.124
1.0	0.179	0.185	0.172	0.168	0.154	0.179
1.2	0.293	0.311	0.287	0.258	0.219	0.293
1.4	0.518	0.542	0.510	0.420	0.299	0.518
1.6	0.623	0.637	0.614	0.549	0.447	0.623
1.8	0.675	0.687	0.667	0.621	0.578	0.675
2.0	0.699	0.711	0.690	0.651	0.619	0.699

Table 3. The RAO of pitch motion

λ/L$_{pp}$	RAO Pitch Motion					
	SEB2	SEB2down	Stern1	Stern2	Basic Form	SEB3
0.5	0.031	0.034	0.028	0.027	0.012	0.031
0.8	0.087	0.089	0.085	0.075	0.025	0.087
1.0	0.162	0.165	0.158	0.145	0.064	0.162
1.2	0.256	0.260	0.250	0.230	0.175	0.256
1.4	0.368	0.370	0.360	0.335	0.280	0.368
1.6	0.467	0.470	0.455	0.430	0.350	0.467
1.8	0.524	0.530	0.510	0.480	0.409	0.524
2.0	0.550	0.560	0.530	0.510	0.441	0.550

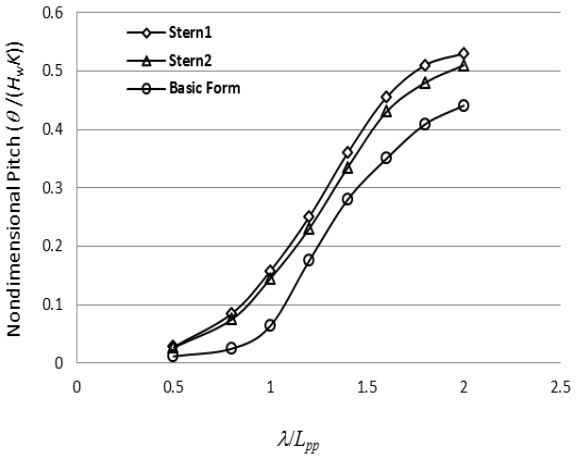

Figure 12 Non-dimensional pitch motions of each stern part improvement

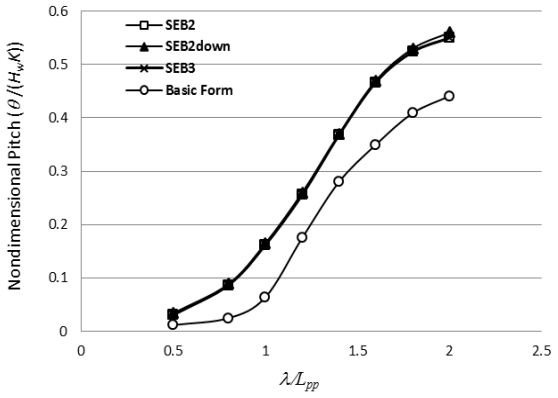

Figure 13 Non-dimensional pitch motions of each addition structure attachment

Meanwhile, the heave amplitudes for SEB2, SEB2down, and SEB3 are close to each other whereas the heave amplitudes for Stern1 and Stern2 are slightly different. Based on Figure 6, SEB2, SEB2down, and SEB3 have slightly different locations for the additional structure attachments. Therefore, the effect on heave motion caused by the attachments is insignificant. The difference between the Stern1 and Stern2 values has been initially presumed to be caused by the part improvement, specifically the improvement of the stern part in the bottom area contributing to good heave amplitude than the one in the side area.

The pitch amplitude for all forms was relatively small and increased with increasing wave length, as shown in Figures 12 and 13. The stern part improvements (Figure 5) and the additional structure attachments (Figure 6) affected an increase on the pitch amplitude by 5% to 9%, depending on the form and the difference value given by the RAO of pitch motion, as shown in Table 3. The form improvements caused displacement or ship mass reduction, where Stern1 modified the rear deck and Stern2 was on the bottom. This form improvement could contribute to the movement of the gravity center point and the gyration radius change. These aspects influenced the pitch motion. Therefore, the Stern2 had a better pitch amplitude compared with the other stern part improvement and the additional structure attachments.

Numerical results are obtained based on interaction between water fluids and fishing boat body, which has an improved stern part form and additional structure attached on its body. The different form of the improved stern part and additional structure attachment has a different of particle number, size, and shape. This numerical method could distinguish even the small size, shape, position, and particle number of an object. Hence, it could calculate fishing boat mass and identify particle as a gravity center point. Therefore, the 3D motions of fishing boat are presented by describing translation and rotation of the gravity center point.

5. CONCLUSION

In this study, the heave and pitch motions of a ship were predicted using a hybrid Eulerian grid with Lagrangian particle scheme. The stern part improvements and the additional structure attachments affected an increase on the heave amplitude from the ship's basic form of 5% to 10%, but the heave amplitude was insignificant if the form differed slightly. Moreover, the improvement of the stern part in the bottom area contributed to a better heave amplitude than the side area improvement. The pitch amplitude for all forms was relatively small and was increased by 5% to 9%, depending on the form. The improvement showed a greater effect on the heave motion than on the pitch motion, but all forms were acceptable based on motion

amplitude. The stern part improvement influenced slight motion response in contrast with resistance reduction. The developed numerical method (Baso et al., 2011a,b; Mutsuda et al., 2013) of a hybrid Eulerian grid with Lagrangian particle could be used practically in the preliminary ship design stage.

6. REFERENCES

Baraff, D., 1997. An Introduction to Physically Based Modelling: Rigid Body Simulation I-Unconstrained Rigid Body Dynamics. *In*: 24th Annual International Conference on Computer Graphics and Interactive Techniques, Special Interest Group on Computer GRAPHics and Interactive Techniques (SIGGRAPH'97) course notes, Los Angeles, August 1997, pp. D1–D31

Baso, S., Mutsuda, H., Doi, Y., 2011a. Numerical Study on Propulsion and Seakeeping Performance of a Ship using a Eulerian Scheme with Lagrangian Particle. *Journal of the Japan Society of Naval Architects and Ocean Engineers*, Volume 13, pp. 19–26

Baso, S., Mutsuda, H., Kurihara, T., Kurokawa, T., Doi, Y., Shi, J., 2011b. A Eulerian Scheme with Lagrangian Particle for Evaluation of Seakeeping Performance of Ship in Nonlinear Wave. *International Journal of Offshore and Polar Engineering*, Volume 21(2), pp. 103–110

Friis, D., Bass, D., Qiu, W., Knapp, C., McGrath, R., Lane, S., 2010. An Overview of Fishing Vessel Efficiency Work in Newfoundland and Labrador, Canada. *In*: The First International Symposium on Fishing Vessel Energy, E-Fishing, Vigo, Spain, May 2010

Friis, D., Knapp, C., McGrath, R., 2017. *Vessel Modification and Hull Maintenance Consideration-options & Pay Back Period or Return on Investments*. Available Online at www.ccfi.ca/pdf/Vessel/.../1Vessel%20Modifications%20and%20Maintenance.pdf, Accessed on November 17, 2018

Gabor, K., 2011. Stern End Bulb for Energy Enhancement and Speed Improvement. *In*: The 11th International Conference on Fast Sea Transportation (FAST2011), Hawaii, USA, pp. 345–354

International Maritime Organization (IMO), 2010. *Emissions from Fuel Used for International Aviation and Maritime Transport. Note by the International Maritime Organization to the thirty-third session of the Subsidiary Body for Scientific and Technical Advice* (SBSTA 33). Available Online at http://www.imo.org/en/OurWork/Environment/PollutionPrevention/AirPollution/Documents/COP%2016%20Submissions/IMO%20Info%20Note%20SBSTA%2033.pdf, Accessed on August 12, 2018

Kawashima, T., Yoshimura, Y., Suzuki, S., Omoto, K., 2003. バルジによる漁船の船型改良について (Improvement of Hull Form of Fishing Vessel by Suitable Bulge). *Journal of the Japan Society of Naval Architects and Ocean Engineers*. Volume 193, pp. 1–9

Kim, H.Y., Yang, C., 2013. Design Optimization of Bulbous Bow and Stern End Bulb for Reduced Drag. *In:* The Twenty-third International Ocean and Polar Engineering Conference, Alaska, USA, Volume 4, pp. 765–772

Kim, H., Yang, C., Noblesse, F., 2010. Hull Form Optimization for Reduced Resistance and Improved Seakeeping via Practical Designed-oriented CFD Tools. *In*: The 2010 Conference on Grand Challenges in Modelling & Simulation (GCMS'10), Ottawa, Canada, pp. 375–385

Legovic, D., Dejhalla, R., 2016. An Overview of Measures for Ship's Energy Efficiency Improvement. *In*: The 22nd Symposium on the Theory and Practice of Shipbuilding, SORTA 2016, Seget Donji, Croatia, pp. 1–12

Masuya, T., 2007. 耐航性 能から み た漁船の 船型改良 (Hull Form Improvement of Fishing Vessels from the View Point of Seaworthiness). *Fisheries Engineering*, Volume 43(3), pp. 193–199

Marine Environment Protection Committee (MEPC), 2011. *Report of the Marine Environment Protection Committee on Its Sixty-Third Session*. Available Online at https://www.mpa.gov.sg/web/wcm/connect/www/61c86de3-4d73-473e-8f40-50c08d41e61d/mepc63-23-report-of-the-mepc-on-its-63rd-session-secretariat.pdf?MOD=AJPERES, Accessed on July 15, 2018

Miyata, H., Doi, Y., 1984. Some Effects of Stern Configurations on Resistance and Propulsion Properties. *Journal of Kansai Soc. Naval Architecture*, Volume 193, pp. 45–52

Miyata, H., Tsuchiya, Y., Inui, T., Adachi, H., 1981. Resistance Reduction by Stern-end Bulb. *Journal of the Japan Society of Naval Architecture and Ocean Engineering*, Volume 19, pp. 16–28

Mutsuda, H., Ishida, A., Baso, S., Doi, Y., 2013. Numerical Investigation of Resistance Reduction of Fishing Boat by Improving Stern Part. *Advanced Shipping and Ocean Engineering*, Volume 2, pp. 77–83

Mutsuda, H., Shinkura, Y., Doi, Y., 2008. A Eulerian Scheme with Lagrangian Particles for Solving Impact Pressure Caused by Wave Breaking. *In*: The 18th International Society of Offshore and Polar Engineers (ISOPE) Conference, Vancouver, Canada, Volume 3, pp. 162–169

Shenglong, Z., Tezdogan, T., Baoji, Z., Leping, X., Yuyang, L., 2018. Hull Form Optimisation in Waves on CFD Technique. *Journal of Ships and Offshore Structures*, Volume 13(2), pp. 149–164

Suastika, K., Hidayat, A., Riyadi, S., 2017. Effects of the Application of a Stern Foil on Ship Resistance: A Case Study of an Orela Crew Boat. *International Journal of Technology*, Volume (8)7, pp. 1266–1275

Supriadi, S., Gunawan, Yanuar, Budhi, H.S., 2015. The Replication of Micro-riblets on Ship Hulls for Drag Reduction Applications. *International Journal of Technology*, Volume 6(6), pp. 983–989

Suzuki, K., Calisal, S.M., Tamashima, M., 1992. 非突出型船首バルブによる漁船船型の改良 (Hull Form Improvement of Fishing Vessel by Non-protruding Bow Bulb). *Journal of the Japan Society of Naval Architects and Ocean Engineers*, Volume 171, pp. 650–651